

Fire, meat and totarol: organic matter in the embankments of the Neolithic site Bastuloken (North Sweden)

JOERI KAAL^{1,2}, JOHAN LINDERHOLM³, AND ANTONIO MARTÍNEZ CORTIZAS⁴

¹Pyrolyscience, Madrid, Spain

²Instituto de Ciencias del Patrimonio (Incipit), Consejo Superior de Investigaciones Científicas (CSIC), Santiago de Compostela, Spain

³Department of Historical, Philosophical and Religious Studies, Umeå University, Umeå, Sweden

⁴EcoPast, Faculty of Biology, Universidade de Santiago de Compostela, Santiago de Compostela, Spain

Compiled September 27, 2019

At the Neolithic site Bastuloken, several subterranean embankments have been identified. The corresponding sediments contain large amounts of bones and lithic elements, indicative of not only massive hunting but possibly also a large (elk) skin processing plant. The present study uses analytical pyrolysis and infrared spectroscopy to track changes in organic matter (OM) composition and relate them to past human activities. It appeared that the sediments contained two layers with a very strong and typical collagen fingerprint (dominated by pyrrole and diketodipyrrole), confirming ubiquitous presence of bone and/or meat. Also, black carbon was abundant in several layers, which indicates presence of nearby fireplaces. Thus far, the results fit with the hypothesis of major inputs of animal tissue especially during two phases recorded between 30–45 cm and 60–65 cm depth, the first of which also contains higher inputs of totarol, indicative of the presence (and probably use) of resin from Cupressaceae (gymnosperm tree). The level of OM preservation in these Neolithic structures is extraordinarily good and shows huge potential for molecular fingerprinting and deepen our understanding of the activities at this important site and the temporary and spatial variability therein.

1. INTRODUCTION

Recently, Linderholm et al. (2019) presented results of a near-infrared (NIR) spectrometry study of the Neolithic site Bastuloken, focusing on methodological aspects such as data evaluation using Principal Component Analysis (PCA) and hyperspectral imaging. They concluded that NIR spectroscopy can be used

for multivariate analysis and obtain meaningful information on archaeological soils and sediments, in terms of understanding site development and soil formation. In the current work, focus is shifted towards the identification of organic matter (OM) constituents in the embankments of the Bastuloken site. For this purpose, we applied Fourier-transform infrared spectroscopy (FTIR) and pyrolysis in combination with gas chromatography and mass spectrometry (Py-GC-MS). Pyrolysis-GC-MS has demonstrated value for molecular characterization of many types of OM, including soil OM, fire residues (black carbon), peat, peat bodies, collagen, paints, and many more (Stankiewics et al., 1997; Kaal et al., 2016), including archaeological deposits (e.g. Shedrinky et al., 1989; Colombini and Modugno, 2009; Kaal and Mailänder, 2018; Kaal et al., 2019). This technique allows for analysis of organic substances with minimal sample pre-treatment requirements, hence it is a rapid screening tool for macromolecular organic substances. FTIR is frequently employed in OM analysis as well (Kögel-Knabner and Rumpel, 2018). It determines the chemical (functional) groups present in a sample and provides less detailed information on molecular structures than Py-GC-MS but, on the other hand, is thought to provide a more complete analysis that is less prone to quantitative and qualitative bias, thus being an adequate complementary tool for Py-GC-MS. We performed FTIR and Py-GC-MS to a sequence of 16 samples from the Bastuloken embankments and evaluated the changes in molecular composition of the OM, in order to identify source material and degradation/preservation state of the organic substances. The ultimate purpose of this exercise is to understand the history of soil development and human activities on the site, and their relationships.

2. MATERIALS AND METHODS

A. Study site and sampling

The Bastuloken site is located in the Ramsele parish in Ångermanland (Sweden; N 63° 40.3622/E 16° 24.1107). The vegetation at and around the site is dominated by pine (*Pinus sylvestris*), lichens and shrub berries (*Vaccinium* spp.). The soils are mainly Podzols developed in a sandy substrate. The sediments in the embankments, i.e. walled structures up to 1 m height (Storå

et al., 2011), contained elk bones, fire-cracked stones and other lithic artefacts (Engelmark and Harju, 2005, Larsson et al., 2012, Linderholm et al., 2013) indicative of large-scale hunting activities. Furthermore, the abundance of bone may be indicative of more than just food production and consumption, such as elk skin processing (Linderholm et al., 2019). These activities may be directly related to the creation of the embankments. Based on radiocarbon dating it has been reported that the sediments cover a period of some 600 yrs in the Late Neolithic (Larsson, 2010; Larsson et al., 2012). The sequence studied here was obtained from a 1x1 m square pit excavation in 2005 (Engelmark and Harju, 2005), with a depth of 80 cm. Samples were obtained at 5 cm intervals ($n=16$), dried and passed through a 2 mm mesh-size sieve, followed by homogenization using a mortar.

B. HF treatment

In order to eliminate minerals that catalyze secondary rearrangements during pyrolysis (dehydration, decarboxylation, cyclization; Schnitzer et al., 1994; Miltner and Zech, 1997; Nierop and Van Bergen, 2002), samples were subjected to mild HF treatment prior to analysis. Briefly, 2.0 g of sample was transferred into 50 ml centrifuge tubes and 10 ml of 1 M HCl was added to remove carbonates. After the reaction was completed, distilled water was added until the 25 ml mark and the suspension was shortly agitated, centrifuged (2500 rpm for 10 min) and the supernatant discarded. Floating root fragments in samples from the surface of the soil (0–30 cm) were removed. Next, 2 % HF solution was added until the 25 ml mark and shaken for 24 hrs, followed by centrifugation and decantation of the supernatant. This HF treatment was repeated five times, after which the procedure was executed three times with H₂O until the 40 ml mark to wash away the remaining acid and fluorosilicates. Finally, the residue was dried at 35 °C. Analogous to harsher HF procedures (Gonçalves et al., 2003; Fang et al., 2010), this treatment has little effect on OM composition (Zegouagh et al., 2004).

C. Analytical pyrolysis

Pyrolysis-GC-MS was performed using a Pt filament coil probe (Pyroprobe 5000) from CDS Analytical (Oxford, USA). The pyrolysis interface was connected to a 6890 GC and 5975 MS from Agilent Technologies (Palo Alto, USA). Approximately 1–1.5 mg of HF-treated sample was embedded in glass wool-containing, fire-polished quartz tubes. Pyrolysis was performed at 750 °C for 10 s (heating rate 10 °C ms⁻¹). The pyrolysis interface and GC inlet were set at 325 °C. The GC oven was heated from 50 to 325 °C at 20 °C min⁻¹ and held isothermal for 5 min. The GC-MS transfer line was held at 325 °C, the ion source (70 eV electron ionisation) at 230 °C and the quadrupole detector at 150 °C. The GC was equipped with a (non-polar) HP-5MS 5% phenyl, 95% dimethylpolysiloxane column (ca. 30 m x 0.25 mm internal diameter; film thickness 0.25 μm). Helium was used as carrier gas (constant flow, 1 ml min⁻¹). For Py-GC-MS, two analytical replicates were obtained. For each pyrolysis chromatogram (or 'pyrogram'), the ca. 50 largest peaks of the total ion current chromatogram were denoted and, if possible, identified. This way, a compound list of 141 pyrolysis products was obtained, which was reduced to 127 compounds after combining overlapping isomers and after omitting compounds that could not be quantified due to co-elution (2-methylfuran, a cyclopentenone, C₁-pyridine, C₂-pyrrole, C₂-phenol, C₂₀-alkene, C₂₀-alkane and C_{18,1} (oleic) acid). The relative proportions of these 127 pyrolysis products were calculated from the peak area of their dominant and/or characteristic mass fragments. Relative proportions are

expressed as the percentage of total quantified peak area (% TQPA), which is a semi-quantitative measure that can be used to compare samples.

D. Fourier transform infrared spectroscopy (FTIR)

Attenuated total reflectance FTIR was performed using a GladiATR (Pike Technologies) spectrometer, scanning in the 4000–400 cm⁻¹ region. In order to compare samples, FTIR signal intensities were normalized to unity. Rough estimations of the relative proportions of major bands were calculated according to maximum peak intensity, if necessary with a baseline subtraction. No replicate analyses were performed. Therefore, statistical comparison between FTIR and Py-GC-MS was based on average results of the two replicates for the latter ($n=16$).

3. RESULTS AND DISCUSSION

A. Pyrolysis-GC/MS: pyrolysis products source allocation

Examples of representative pyrograms are presented in Figure 1a.

Carbohydrates. The pyrolysis products assigned to the carbohydrate component group were 3/2-furaldehyde, 5-methyl-2-furaldehyde, 4-hydroxy-5,6-dihydro-(2H)-pyran-2-one, 1,4:3,6-dianhydro-D-glucopyranose, dianhydrorhamnose, levoglucosenone, levoglucosan and an unidentified compound with a similar mass spectral pattern, peak shape and depth trend as 1,4:3,6-dianhydro-D-glucopyranose but with shorter retention time. These compounds originate from plant-derived polysaccharides in different states of decay and microbial carbohydrates (Pouwels et al., 1989) and account for 24 ± 12 % of TQPA. The contribution of these compounds decreases with depth ($r^2=0.73$, $P<0.001$), from ca. 45 % at the surface to ca. 15 % at the bottom of the profile (Fig. 2a). Levoglucosan is the most abundant carbohydrate-derived pyrolysis product, accounting for 80 % of the carbohydrates in the top 30 cm and ca. 40 % in the deeper layers. The significant contributions of levoglucosan in this millennia-yr old soil suggests that a stabilization mechanism (such as a combination of metal binding, occlusion and cold/wet conditions) operates on the OM, as levoglucosan is a marker of relatively intact cellulose (Poirier et al., 2005) that typically disappears during the transformation of living biomass into soil OM under aerobic conditions. The compounds 3/2-furaldehyde (19 ± 6 % of total carbohydrates) and 5-methyl-2-furaldehyde (9 ± 5 %) have, after levoglucosan, the highest average contributions to the carbohydrates. These products may originate from both intact as well as degraded or microbial carbohydrates including chitin. In the present study, the interpretation of the source of levoglucosenone (1.1 ± 0.7 % of TQPA) is ambiguous, as it may originate from chitin and its derivatives (Van der Kaaden, 1984), from partially degraded carbohydrates (e.g. Marbot, 1997) as well as from acid-catalyzed cellulose dehydration reactions during pyrolysis (Browne, 1958).

Nitrogen-containing compounds. Pyrolysis products containing one or two atoms of N accounted for 22 ± 14 % of TQPA. Apart from the major variations in the summed proportion of N-containing compounds with depth (Fig. 2b), the dominant member of these compounds changes strongly within the profile. Surprisingly, the second most abundant N-containing pyrolysis product is diketodipyrrole (4 ± 5 % of TQPA; 12 ± 9 % of the N-containing compounds), which is rare in Py-GC-MS of soil OM.

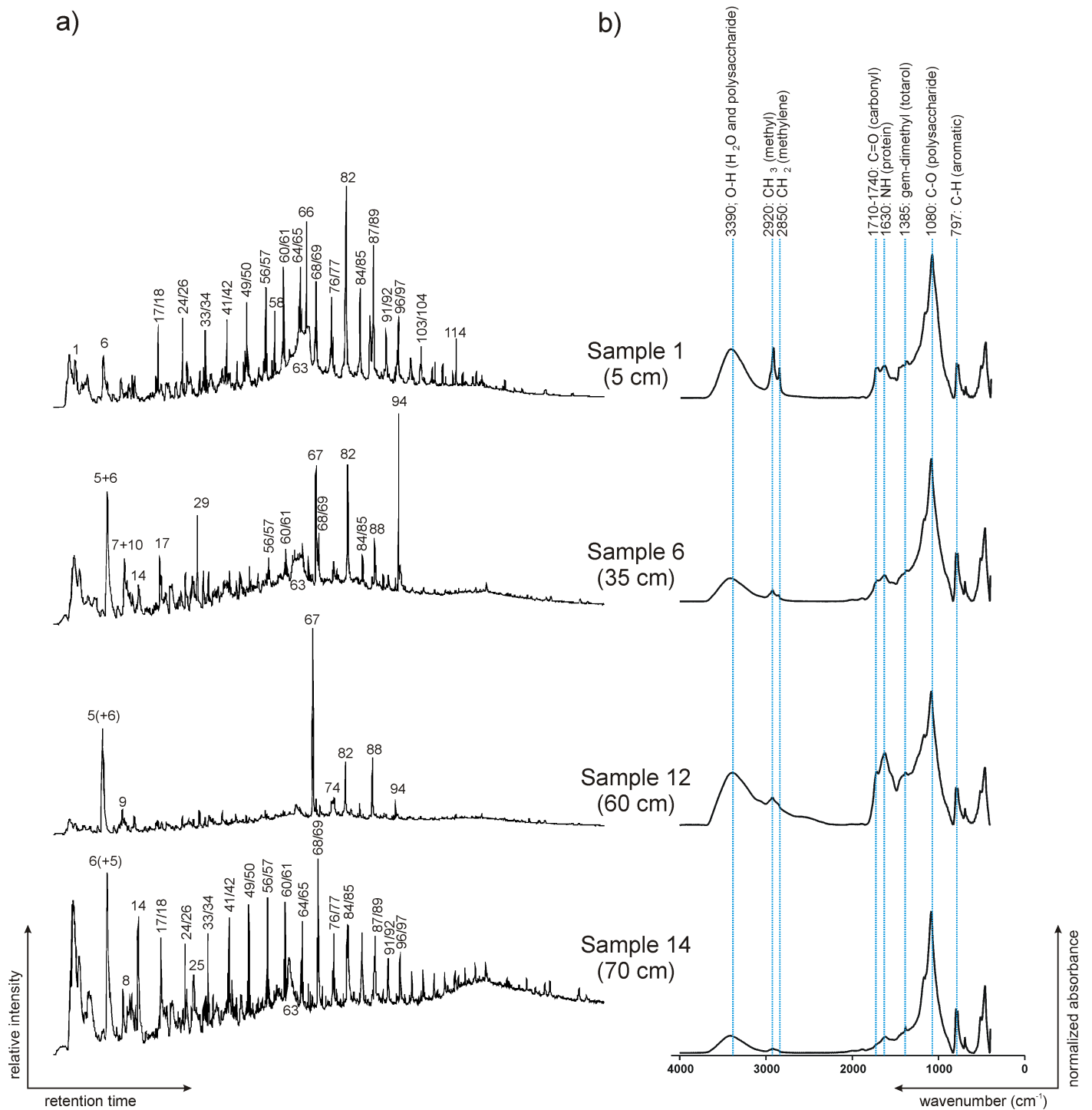


Fig. 1. Examples total ion current chromatograms from Py-GC-MS (a) and absorbance spectra from FTIR (b) of selected samples. For Py-GC-MS, peak labels refer to compound numbers in Table 1 (see the end of the document).

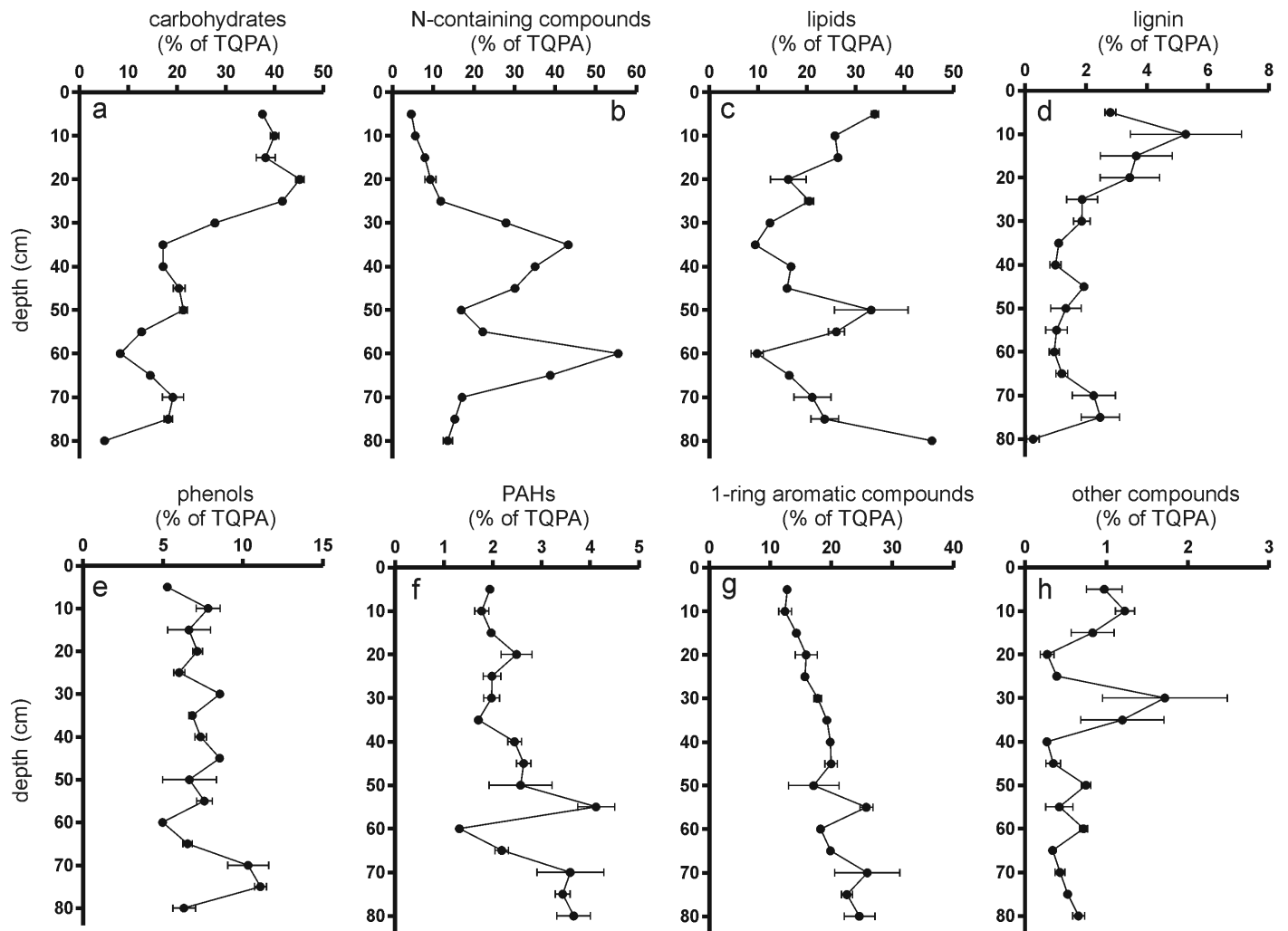


Fig. 2. Relative proportions of the main pyrolysis product groups, expressed as % of TQPA, and their changes with depth in the Bastuloken sediment sequence. Error bars represent standard error of two analytical replicates. PAHs = polycyclic aromatic hydrocarbons.

Diketodipyrrole is a dimerization product of HYP-HYP (hydroxyproline) peptide linkages in proteinaceous biomass (Van Bergen et al., 1998; Chiavari and Prati, 2003; Chiavari et al., 2003). In the present study, two buried layers (30–45 cm and 60–65 cm) provided exceptionally high proportions of diketodipyrrole (up to 17 % of TQPA at 60 cm) and not of any other markers of fresh vegetation remains, which eliminates the possibility of a significant production of diketodipyrrole from plant pigments or vegetal proteins. Of the diketopiperazines that are often observed in pyrograms (see e.g. Smith et al., 1988), the compound producing m/z 194 and 70, which probably originates from PRO-PRO (proline) dimerization and intermolecular condensation reactions of PRO during pyrolysis (Choi and Ko, 2010; Fabbri et al., 2012a), was the most abundant. This diketopiperazine (0.3 ± 0.2 % of TQPA), but also the less specific N-containing compounds pyrrole (5 ± 4 %) and C_1 -pyrroles (3.5 ± 2.1 %), are strongly enriched in the layers with exceptionally high diketodipyrrole proportions (see example Fig. 2a). Similarly, the pyrolysis fingerprints of animal glue analysed by Chiavari and Prati (2003) and Chiavari et al. (2006) were dominated by pyrrole, C_1 -pyrroles and diketodipyrrole. This molecular evidence shows the presence of HYP- and PRO-enriched protein that can only be ascribed to collagen (Fabbri et al., 2012b; Kaal et al., 2016; Cersoy et al., 2018). Some minor unidentified N-containing pyrolysis products showed a similar distribution in the soil as the compounds described above ($P < 0.001$): a polar N-containing compound giving m/z 92 and 65 (pyrrole carbonitrile), a possible oxazoline compound (m/z 94 and 185), m/z 200 and 199 (three isomers, possibly of methylthiazoloquinolines), a compound with dominant masses m/z 171 and 172 and a compound producing mainly m/z 176 and 154. The compound giving dominant m/z 171 and 172 may have been present in the pyrolyzates of chitin-rich soils from the Azores Islands studied by Nierop et al. (2005), in an archaeological bog body tissue studied by Stankiewicz et al. (1997) who identified it as 5-hydroxy-4-phenylpyrimidine, and from collagen extracted from archaeological bones (Fabbri et al., 2012b; Adamiano et al., 2013; Kaal et al., 2016; Cersoy et al., 2017). Therefore, it is concluded that the majority of these other N-containing pyrolysis products, and particularly those that provide maximum contributions in the two buried layers at 30–45 cm and 60–65 cm, originate from animal protein as well. These two layers coincide with macroscopic bone fragments (Linderholm et al., 2019). Therefore, the N fingerprint strongly indicates that a significant proportion of the OM (reflected by 15–50 % of TQPA) in six bone-rich samples between 30 and 45 cm and 60 and 65 cm depth originates from HYP- and PRO-dominated proteins from animal tissue, such as the structural component of bone collagen (including cartilage) and ligaments and tendons (meat). Arguably, this study represents the most unambiguous example of molecular detection of ancient collagen from an archaeological site, and the fact that the materials are as old as the Neolithic makes it even more surprising to find such well-preserved collagen fingerprints (see also Fig. 1a, 35 cm and 60 cm depth chromatogram examples).

Benzonitrile (1.0 ± 0.6 % of TQPA) is often reported to originate primarily from pyrogenic material (black carbon; Kaal and Rumpel, 2009; Kaal et al., 2009; Song and Peng, 2010; Suárez-Abelenda et al., 2017), although it cannot be excluded that it may sometimes originate from intact non-charred partially degraded OM (Boon, 1984; Alcañiz et al., 1987; Song and Farwell, 2004; Buurman et al., 2009; Bonmatí et al., 2009). Indeed, the depth profile of this compound follows ($P < 0.001$) that of the non-alkylated polycyclic aromatic hydrocarbons (PAHs; see be-

low), which probably originate from pyrogenic OM (Rumpel et al., 2007). The C_1 -benzonitriles, which account for 0.8 ± 0.4 % of TQPA, are closely related to benzonitrile ($r^2 = 0.83$, $P < 0.001$), which suggests that these compounds originate from pyrogenic OM (see also Schnitzer et al., 2007) rather than uncharred protein. Benzonitrile and methylbenzonitriles combined account for 8 ± 3 % of the N-containing compounds. Indole (0.6 ± 0.2 % of TQPA) and pyridine (3.4 ± 1.4 %) are correlated ($P < 0.001$) to the sum of benzonitriles, but these products are less specific for pyrogenic OM; indole and pyridine are often associated with relatively intact proteinaceous biomass and microbial biomass, respectively (Suárez-Abelenda et al., 2011).

Chitin, a *N*-acetylglucosamine-based polymer, is reflected in the pyrolyzates by acetamide (1.2 ± 0.5 %), which is one of the most important pyrolysis products of chitin (Stankiewicz et al., 1996, 1997; Bierstedt et al., 1998) while several smaller peaks of other chitin markers such as the acetomidosugars (compounds giving typical fragments m/z 109, 111, 137, 139, 153 and 167; see e.g. Stankiewicz et al., 1998) were detectable but were not recognized in the initial screenings of the pyrolyzates and therefore not quantified. In the present study, the chitin originates from fungal cell walls and/or arthropod exoskeletons. An unidentified N-containing compound producing mainly m/z 95 is correlated with the proportion of acetamide ($P < 0.001$). This could be a chitin product as well (Stankiewicz et al., 1996). A series of linear N-containing aliphatic compounds were detected (C_{16} - and C_{18} -alkylnitrile and C_{16} - and C_{18} -alkylamide). These aliphatic compounds, the sum of which contributes only 0.5 ± 0.2 % of TQPA, tend to be concentrated in the deeper layers of the soil, and probably originate from microbial organic matter.

Methylene chain aliphatic compounds. Homologous series of aliphatic pyrolysis products (*n*-alkanes, *n*-alkenes, fatty acids and 2-methylketones) are from hereon referred to as methylene chain compounds (MCC). In addition, a series of plant sterols, prist-1-ene and some unidentified aliphatic compounds were allocated to this component group. The sum of these compounds accounts for 22 ± 10 % of TQPA, the vast majority of which is accounted for by the *n*-alkane/*n*-alkene pairs (C_6 – C_{33}). The sum of MCC decreases linearly ($r^2 = 0.87$; $P < 0.001$) from ca. 35 % of TQPA at the surface towards 10 % at 35 cm depth (Fig. 2c). Below this depth, this sum is negatively correlated ($r^2 = 0.58$; $P < 0.001$) to the sum of N-containing compounds: the proportion of MCC shows minimum levels in the two layers that contain large amounts of probably animal tissue (14 ± 5 % at 25–45 cm and 13 ± 4 % at 60–65 cm depth) and maximum levels in between these layers (30 ± 8 % at 50–55 cm) and the bottom of the profile (31 ± 5 % at 70–80 cm). Therefore, except for the surface of the soil, where relatively intact plant material is present (lignin and polysaccharides), the proportion of total MCC depends primarily on source material (animal tissue versus degraded and perhaps root-derived OM). The *n*-fatty acids show a different general depth pattern than the general trend described above. The C_{16} – C_{22} -fatty acids (3 ± 1 % of TQPA; 14 ± 7 % of total MCC) are concentrated in the surface of the soil (positive correlation with levoglucosan from intact cellulose; $r^2 = 0.60$; $P < 0.001$). Prist-1-ene follows this pattern: a significant decline from 1.3 % to less than 0.2 % of TQPA in the upper 30 cm of the soil ($r^2 = 0.66$; $P < 0.01$) and proportions below 0.3 % in deeper layers. Prist-1-ene probably originates from the phytol side-chain of chlorophyll or tocopherol, which explains its highest level in the top layers of the soil where relatively intact plant material is concentrated. The C_{22} – C_{31} -methylketones (0.8 ± 0.5 % of TQPA;

4 ± 1 % of total MCC) showed a strong odd-over-even predominance. A series of plant sterols (probably stigmasta derivatives), together accounting for 0.4 ± 0.3 % of TQPA, showed highest contributions in the layers at 50–55 and 70–80 cm depth, but they were negligible in the surface of the soil. Preservation of plant sterols depends strongly on the water regime of the soil in which it is stored (Schellekens et al., 2009). Perhaps the layers below ca. 40 cm had been water-logged for most of the time after it was buried. This would also explain the abundance of levoglucosan in the deeper layers of the soil and the exceptional preservation of proteinaceous biomass (cf. Stankiewicz et al., 1997).

Lignin. Lignin was recognised by a series of methoxyphenols. In the present study, eight methoxyphenolic compounds were identified, all of them based on the guaiacol (2-methoxyphenol) moiety. Their sum amounts to 11 ± 4 % of TQPA. Syringol moieties were absent, suggesting that all or most lignin originates from coniferous species (softwood forest). The proportion of the sum of the lignin markers decreases from ca. 5 % at the surface towards levels below 1 % at the bottom of the sequence (negative linear depth trend: $r^2=0.35$, $P<0.001$) (Fig. 2d). Within this component group, guaiacol is the most abundant product (31 ± 11 % of the sum of lignin compounds), followed by 4-vinylguaiacol (29 ± 8 %). The contribution of lignin markers with a C_3 -side chain (propyl or propylene) is 11 ± 4 %, and there is no significant depth trend of the proportion of C_3 -guaiacols, suggesting that there is no significant C_3 -side chain oxidation after burial, which probably is a result of predominantly anaerobic OM storage conditions.

Phenols. Phenol and alkylated phenols (methylphenols and C_2 -phenols) account for 7 ± 2 % of TQPA. The proportion of phenol (3.3 ± 0.9 % of TQPA) increases gradually with depth ($r^2=0.36$, $P<0.001$) (Fig. 2e). Within the phenols group, phenol (45 ± 6 % of total phenols) and 4-methylphenol (40 ± 4 %) are the dominant compounds. The proportion of phenol (of total phenols) increases with depth ($r^2=0.56$, $P<0.001$) and the relative contributions of the other phenols decrease significantly with depth ($P<0.001$). The phenols originate from many biocomponents including proteins, polysaccharides and lignin, and their weakly charred counterparts, which makes it difficult to interpret these compounds. On the other hand, the sum of lignin products closely follows that of 4-methylphenol ($r^2=0.82$; $P<0.001$) and C_2 -phenol ($r^2=0.46$; $P<0.001$), suggesting that lignin is an important source of at least some of the phenols.

Polycyclic aromatic hydrocarbons. The PAHs account for 2.5 ± 0.9 % of TQPA. The contribution of PAHs fluctuates around 2 % of TQPA in the top 35 cm, then increases to more than 4 % at 55 cm, followed by a strong decrease to less than 1.5 % at 60 cm and finally a gradual increase towards 4 % in the bottom layers of the soil (Fig. 2f). The most common source of these compounds is pyrogenic OM (e.g. Ross et al., 2005; Rumpel et al., 2007), although analytical pyrolysis may induce artificial formation of PAHs (Sáiz-Jiménez, 1995), raising caution. Minerals that might cause such secondary rearrangements, especially the cyclization of aliphatic moieties, are assumed to have been largely eliminated during HF treatment. Indeed, quartz was the only mineral that could be identified from the FTIR spectra (see below), and quartz is known to have a negligible effect on pyrolysis reactions (Miltner and Zech, 1997). Furthermore, our experience is that mineral-induced artificial charring produces relatively large amounts of long-chain alkylbenzenes (C_4 – C_{23})

and alkyl-PAHs, and relatively low proportions of benzene and non-alkylated PAHs. The opposite is observed in the present study. Therefore, it is more than likely that the PAHs originate from pyrogenic OM that formed during domestic- and/or wildfires. Charcoal fragments were identified using the light microscope, providing support for this interpretation (Figure 4).

Monocyclic aromatic hydrocarbons. The MAHs benzene, toluene and C_2 -benzenes may originate from diverse precursors (Alcañiz et al., 1987) and therefore the presence of these compounds cannot be used directly to infer the presence of any specific biocomponent. However, using Py-GC-MS literature and correlation analysis some information can be extracted from them, which account for 19 ± 5 % of TQPA (Fig. 2g). Benzene accounts for 2.7 ± 1.1 % of TQPA. Benzene closely follows PAHs contribution ($r^2=0.85$; $P<0.001$), suggesting that pyrogenic OM is the main source of benzene (Braadbaart and Poole, 2008; Kaal and Rumpel, 2009). The C_2 -benzenes (styrene, dimethylbenzenes and ethylbenzene) account for 4.8 ± 1.5 % of TQPA. These compounds are correlated with PAHs content ($r^2=0.84$; $P<0.001$), suggesting that they originate largely from pyrogenic OM as well. On the contrary, toluene (11 ± 3 % of TQPA) is not correlated to the PAHs or benzene contribution, probably because of the strong production of toluene from the pyrolysis of protein and degraded soil OM (Buurman et al., 2009). In Py-GC-MS studies of pyrogenic OM-rich colluvial soils from NW Spain toluene showed similar depth trends as benzene, benzonitrile and PAHs, and was therefore concluded to originate largely from pyrogenic OM (Kaal et al., 2008a/b). However, the pyrogenic OM content of the OM in these soils from NW Spain is much higher than is the case for the sequence studied here, while protein-derived biomass is exceptionally abundant in the pyrolyzates of the present study, and therefore in the Bastolukén embankment toluene should be largely ascribed to proteinaceous biomass.

Other compounds. Remaining products account for 0.7 ± 0.5 % of TQPA (Fig. 2h). A pyrolysis product producing fragment ions m/z 271 (100 %), m/z 175 (73 %), m/z 201 (52 %), m/z 286 (M^+ ; 37 %), m/z 189 (34 %), m/z 272 (22 %), m/z 69 (18 %), m/z 159 (16 %), m/z 202 (13 %) and m/z 176 (11 %) was identified as totarol. Totarol is a diterpene phenolic compound that was first isolated from *Podocarpus totara* (Podocarpaceae) resins and, later, from various species in the Cupressaceae family (e.g. Constantine et al., 2001; Sharp et al., 2001). Podocarpaceae only occur in the Southern Hemisphere. As far as we know, totarol has not been documented in the Py-GC-MS literature of soil OM. Chiavari et al. (1995) and Peris Vicente (2008) detected totarol in the pyrolyzates from sandarac resin obtained from species from the Cupressaceae family. Juniper resins have also been identified as a frequent source of totarol (Mills and White, 1994). Totarol contributes only 0.4 ± 0.5 % to the TQPA, with a maximum between 30–35 cm (1 % of TQPA; but note that this sharp peak is actually the highest intensity at 35 cm; Fig. 1a chromatogram of sample at 35 cm depth, compound 94) and a second smaller maximum at 60 cm (0.5 % of TQPA). Therefore, maximum levels in totarol contribution coincide with the layers enriched in bone material and animal protein. Finally, a 4*H*-naphthalene compound (m/z 159 and 177) was detected in the surface of the soil (0.4 % of TQPA) (not shown). The contribution of this compound declines towards below 0.1 % of TQPA at 15 cm depth. This compound may originate from a resin that is either rapidly degraded, leached from the soil or restricted to recent vegetation,

for example from pine resin (hydronaphthalenes are not group with PAHs for its predominant source in terpenoids).

B. FTIR

Example spectra can be found in Fig. 1b and the relative proportions of selected bands in Fig. 3. A broad band at ca. 3390 cm^{-1} (Fig. 3a) originates mainly from O-H groups in water and polysaccharides. Aliphatic CH_2 and CH_3 stretches between 3000 and 2850 cm^{-1} decline with depth (Fig. 3b/c), analogous to the MCC in pyrolyzates. The ratio of CH_2/CH_3 , reflecting the relative proportion of terminal CH_3 and in-chain methylene CH_2 and thus a measure of chain length, increases with depth (not shown; $r^2=0.62$, $P<0.001$), which reflects preferential degradation of long-chain "fresh" methylene chain compounds relative to shorter chain structures, especially in the top 40 cm of the soil. The depth trends for the bands at $1740\text{--}1710\text{ cm}^{-1}$ (Fig. 3d) and 1630 cm^{-1} (Fig. 3e), respectively from carbonyl $\text{C}=\text{O}$ and amine N-H , are enriched in the layers that are enriched in proteinaceous animal tissue ($P<0.01$). In the upper layers of the soil, a significant portion of the carbonyl $\text{C}=\text{O}$ does not correspond to amide but probably carboxylic groups in lignin. The peak of the mainly amine N-H bend shifted between 1630 and 1610 cm^{-1} , possibly because of variations in the contribution of aromatic $\text{C}=\text{C}$ stretches, from lignin at the surface of the soil and pyrogenic OM in the deeper layers. Band overlap makes it difficult to interpret the FTIR results in this region. A small but easily recognized sharp band at 1385 cm^{-1} (Fig. 3f), probably of gem-dimethyl groups, supports the presence of totarol or a similar compound (Bennett and Cambie, 1966; Coates, 2000). The relative proportion of this group is correlated to totarol as determined by Py-GC-MS ($P<0.001$). The broad band corresponding to the polysaccharide C-O stretch at 1080 cm^{-1} (Fig. 3g) shows a similar depth trend as the sum of carbohydrate markers from Py-GC-MS, with the exception of the bottom of the profile. A combination of aromatic C-H vibrations (Fig. 3h) coincides with the sum of lignin and pyrogenic OM (from Py-GC-MS), with lignin being dominant until 35 cm and pyrogenic OM in the bottom part of the profile. Finally, a band of unknown source at 1165 cm^{-1} coincides with total MCC from Py-GC-MS. In conclusion, these results coincide well with those of Py-GC-MS.

C. Soil formation and archaeological implications

The most striking feature observed by OM characterization of the Bastuloken soil is the existence of two layers in which the soil OM consists largely of intact animal protein, probably from bone or meat collagen. Figure 4a shows the sum of the pyrolysis products that are most specific of these proteins (diketodipyrrole, diketopiperazine and the compounds tentatively identified as carbonitrilepyrrole, an oxazoline compound, 5-hydroxy-4-phenylpyrimidine and methylthiazoloquinolines). This figure is more representative of the proportion of animal protein than the sum of all N-containing compounds (Fig. 2b) as bias from N groups in vegetal protein and pyrogenic OM is avoided. This explains the very low "baseline" levels for the first 25 cm and the last 10 cm of the sampled embankment. Maximum levels are found at 30-45 cm and 60-65 cm depth, which coincides with largest amounts of bone remains at 30-40 (1,2 kg obtained during excavation of the 1x1 m pit) and 60 cm depth (2,2 kg) (Linderholm et al., 2019). The material between these two layers (50-55 cm) has lower proportions of animal protein and enhanced levels of pyrogenic OM (Fig. 4f), indicative of shifts in local activities (use of fire, elk processing, etc.) that need further investigation

and refined chronological information. The lower and upper layers of the deposit are useful for testing baseline levels of proxies related to animal protein inputs.

Even though furaldehydes in pyrolyzates originate from both degraded as well as intact polysaccharides, the ratio of levoglucosans to furaldehydes can often be used as an indication of the degradation state of the carbohydrates (Schellekens et al., 2009). Figure 4b shows the contribution of levoglucosan to total carbohydrates. The depth trend of this ratio suggests that the more intact carbohydrates are found in the top 20 cm. The proportion of levoglucosan remains around 40 % below that layer, which is remarkably high for millennia-yrs-old soil OM from mineral soils. Perhaps the soil had been waterlogged during most of its formation period. Similar to levoglucosan from relatively intact polysaccharides, the C_3 -guaiacols from intact lignin are often rapidly aerobically degraded in mineral soils. Figure 4c shows the proportion of guaiacol moieties with a C_3 side-chain, as a percentage of total guaiacol contribution. This proportion can be used as an indicator of aerobic oxidation in peat profiles. It fluctuates around 10-15 %, suggesting that aerobic decay had little effect on lignin composition.

Figure 4d shows the proportion of totarol (% of TQPA). Maximum values in totarol concentration coincide with the protein-rich layers of the soil. This may point towards a relationship between that particular phase of animal tissue processing/production/consumption and use of Cupressaceae or reflect the forest environment during that phase. If future research points out that the former is the most most likely cause of coetaneous peaks in collagen and Cupressaceae resin, the use of totarol as an antibacterial agent (against mycobacteria such as *Mycobacterium tuberculosis*; Constantine et al., 2001), must be considered. Gordien et al. (2009) found totarol to be the most efficient antimycobacterial agent among a variety of Cupressaceae terpenoid products. At this point it would be speculation to ascribe the peaks in totarol content at 30-35 cm and 60 cm to application as an anti-pathogen by the people that were processing the elk meat and perhaps skins at the site, but it would be similarly speculative to assign these observations to the most plausible alternative explanation (enhanced input of Cupressaceae litter) as guaiacyl lignin proportions are very low in these levels.

Figure 4e presents the depth profile of acetamide (% of TQPA). Acetamide shows low levels at the surface ($<0.5\%$), increased towards $>2\%$ at 30 cm depth and then gradually declines to ca. 1 % at the bottom of the sequence. This trend reflects the unscathed plant-derived biomass at the surface (low chitin concentration) and input of microbial biomass below 30 cm (producing chitin). There is no support of a major abundance of skeletal remains from scavenging arthropods in the layers that contain large proportions of protein-derived biomass, which were interpreted as being the "archaeological layers". These results may point towards a much lower (or no) anthropogenic influence on OM composition during the phase that corresponds to deposit formation at 0-20 cm depth (remember, the embankments are buried; the least deep sample corresponds to the late Neolithic) or that posterior penetration and incorporation to the OM of roots overshadowed the signal of anthropogenically-driven inputs.

Figure 4f shows the sum of those pyrolysis products that largely originate from pyrogenic OM. This figure provides a rough estimation of the proportion of fire-derived biomass in the Bastuloken soil. We have no convincing rationalization for the changes in fire residue proportions with depth, but a recurrent use of fire is considered likely. Figure 5 shows photographs of

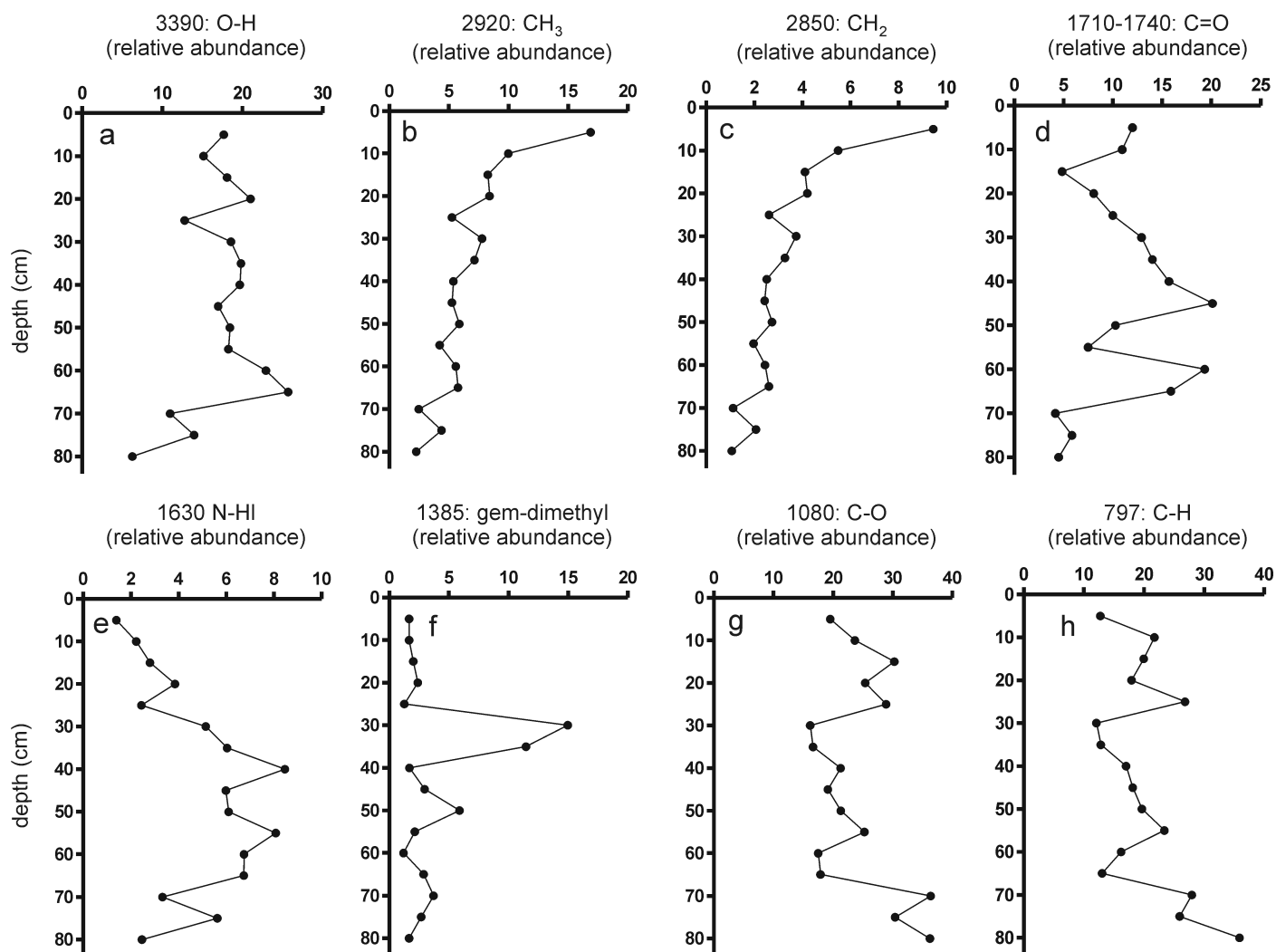


Fig. 3. Relative proportions of specific FTIR bands used for tracking changes with depth in the Bastuloken sediment sequence (based on peak heights after baseline subtraction).

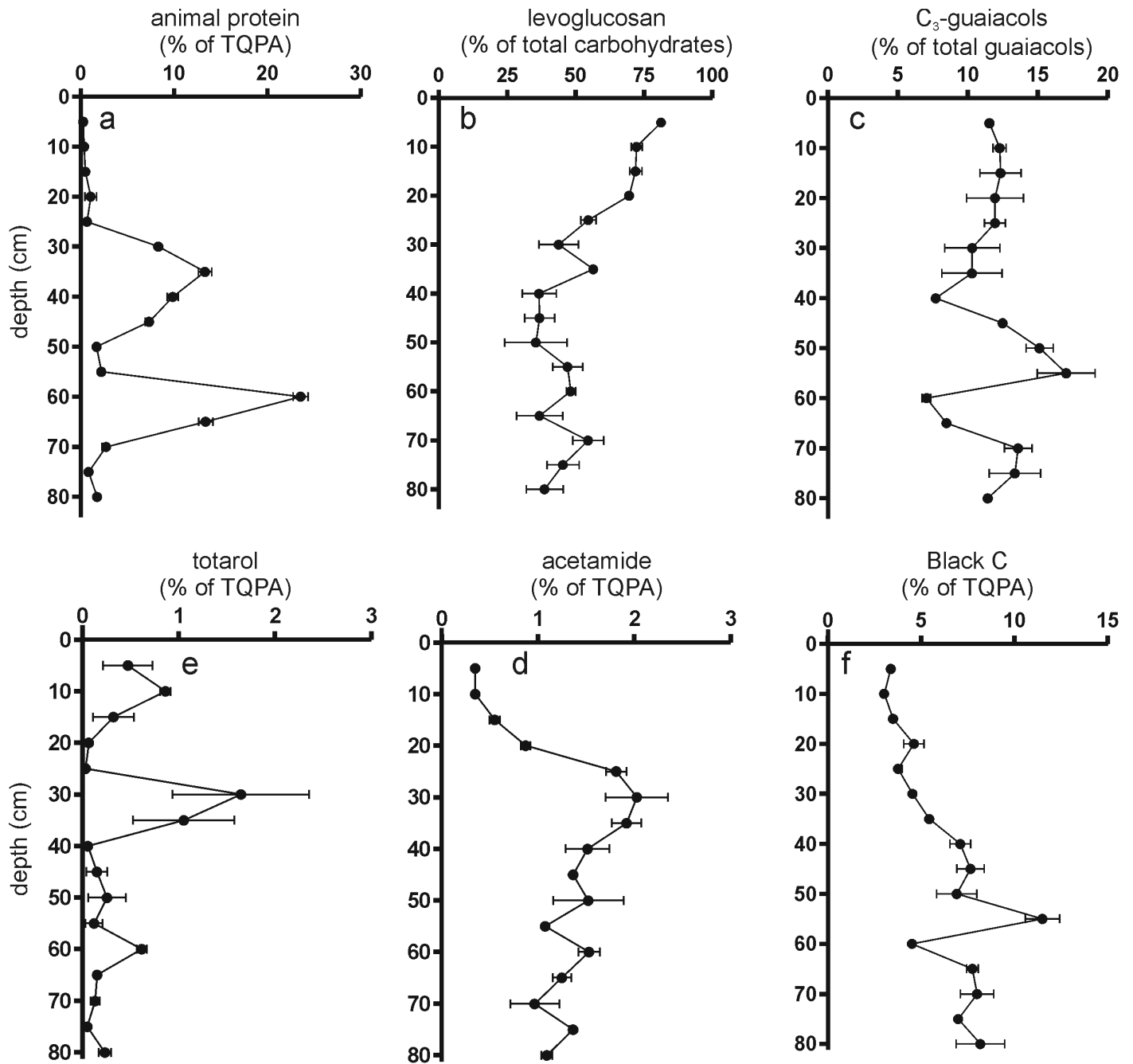


Fig. 4. Markers and proxies of specific OM sources and decay processes, after Py-GC-MS. Error bars represent standard error of two analytical replicates.

pyrogenic-rich material from the Bastuloken sequence analyzed in the present study, confirming the presence of fire residues.

4. CONCLUSIONS

The molecular characterization of the samples from the Bastuloken sequence show the presence of three types of OM that are probably related to anthropogenic activities, i.e. (1) collagen from animal tissue (meat/bone), (2) totarol from diterpenoid resin (not pine; probably Cupressaceae) and (3) pyrogenic OM from fire residues. Most of the anthropogenic materials show maxima at 30-45 cm and 60-65 cm depth, which are the layers that are most likely to have formed coetaneously with the period of most intense use (link with elk bone abundance). Natural edaphic processes are reflected by chitin (fungi/arthropods, possible scavengers of anthropogenic residues), lignin, some root-derived aliphatic OM and intact polysaccharides, most of which are enriched in surface layers. FTIR and Py-GC-MS are complementary tools that have a clear potential to unravel the history of archaeological deposits with such excellent preservation conditions as is the case for Bastuloken.

5. REFERENCES

Adamiano, A., Fabbri, D., Falini, G., Belcastro, M.G., 2013. A complementary approach using analytical pyrolysis to evaluate collagen degradation and mineral fossilisation in archaeological bones: The case study of Vicenne-Campochiaro necropolis (Italy). *Journal of Analytical and Applied Pyrolysis* 100, 173-180.

Alcañiz, J.M., Cabeza, L., Comellas, L., Gassiot-Matas, M., Serés, A., 1987. Comparative identification of pyrolysis products from soil organic matter and some plant debris. In: Giovannozzi-Sermani, G., Nannipieri, P. (Eds.), *Current perspectives in environmental biogeochemistry*. VII International Symposium on Environmental Biogeochemistry, Rome 1985, pp. 35-46.

Bennett, CR, Cambie, RC, 1966. Chemistry of the podocarpaceae—XI: Reductions of totarol. *Tetrahedron* 22, 2845-2860.

Bierstedt, A., Stankiewicz, B.A., Briggs, D.E.G., Evershed, R.P., 1998. Quantitative and qualitative analysis of chitin in fossil arthropods using a combination of colorimetric assay and pyrolysis-gas chromatography-mass spectrometry. *Analyst* 123, 139-145.

Bonmatí, M., Ceccanti, B., Nannipieri, P., Valero, J., 2009. Characterization of humus-protease complexes extracted from soil. *Soil Biology and Biochemistry* 41, 1199-1209.

Boon, J.J., 1984. Tracing the origin of chemical fossils in microbial mats: biogeochemical investigations of Solar lake cyanobacterial mats using analytical pyrolysis methods. In: Y. Cohen, R.W. Castenholz and H.O. Halvorson (eds.), *Microbial Mats: Stromatolites*, Alan R. Liss, New York, pp. 313-342.

Braadbaart, F., Poole, I., 2008. Morphological, chemical and physical changes during charcoalification of wood and its relevance to archaeological contexts. *Journal of Archaeological Science* 35, 2434-2445.

Browne, F.L., 1958. Theories of the combustion of wood and its controls. Report No. 2136 of the Forest Products Laboratory Madison, Madison. 72 pp.

Buurman, P., Nierop, K.G.J., Kaal, J., Senesi, N., 2009. Analytical pyrolysis and thermally assisted hydrolysis and methylation of EUROSIL humic acid samples - A key to their source. *Geoderma* 150, 10-22.

Cersoy, S., Daheur, G., Zazzo, A., Zirah, S., Sablier, M., 2018. Pyrolysis comprehensive gas chromatography and mass spectrometry: A new tool to assess the purity of ancient collagen prior to radiocarbon dating. *Analytica Chimica Acta* 1041, 131-145.

Chiavari, G., Prati, S., 2003. Analytical pyrolysis as diagnostic tool in the investigation of works of art. *Chromatographia* 58, 543-554.

Chiavari, G., Fabbri, D., Mazzeo, R., Bocchini, N., Galletti, G.C., 1995. Pyrolysis gas chromatography-mass spectrometry of natural resins used for artistic objects. *Chromatographia* 41, 273-281.

Chiavari, G., Lanterna, G., Luca, C., Matteini, M., Prati, S., Sandu, I.C.A., 2003. Analysis of proteinaceous binders by in situ pyrolysis and silylation. *Chromatographia* 57, 645-648.

Chiavari, G., Fabbri, D., Galletti, G.C., Prati, S., Scianna, N., 2006. Use of pyrolysis-gas chromatography/mass spectrometry to characterise binding media and protectives from a Coronelli's terrestrial globe. *Journal of Cultural Heritage* 7, 67-70.

Choi, S.S., Ko, J.-E., 2010. Dimerization reactions of amino acids by pyrolysis. *Journal of Analytical and Applied Pyrolysis* 89, 74-86.

Coates J., 2000. Interpretation of infrared spectra, a practical approach. *Encyclopedia of Analytical Chemistry*, R.A. Meyers (Ed.), John Wiley Sons Ltd, Chichester, 10815-10837.

Colombini, M.P., Modugno, F., 2009. *Organic Mass Spectrometry in Art and Archaeology*. John Wiley Sons, Ltd, Chichester.

Constantine, G.H., Karchesy, J.J., Franzblau, S.G., LaFleur, L.E., 2001. (+) - Totarol from *Chamaecyparis nootkatensis* and activity against *Mycobacterium tuberculosis*. *Fitoterapia* 72, 57-574.

Engelmark, R., Harju, J., 2005. Rapport över arkeologisk förundersökning av Raä 183, Ramsele sn, Ångermanland, 2005. Umeå: Institutionen för arkeologi och samiska studier, Umeå universitet.

Fabbri, D., Torri, C., Spokas, T.A., 2012a. Analytical pyrolysis of synthetic chars derived from biomass with potential agronomic application (biochar). Relationships with impacts on microbial carbon dioxide production. *Journal of Analytical and Applied Pyrolysis* 93, 77-84.

Fabbri, D., Adamiano, A., Falini, G., Marco, R., Mancini, I., 2012b. Analytical pyrolysis of dipeptides containing proline and amino acids with polar side chains. Novel 2,5-diketopiperazine markers in the pyrolysates of proteins. *Journal of Analytical and Applied Pyrolysis* 95, 145-155.

Fang, X., Chua, T., Schmidt-Rohr, K., Thompson, M.L., 2010. Quantitative ¹³C NMR of whole and fractionated Iowa Mollisols for assessment of organic matter composition. *Geochimica et Cosmochimica Acta* 74, 584-598.

Gonçalves, C.N., Dalmolin, R.S.D., Dick, D.P., Knicker, H., Klamt, E., Kögel-Knabner, I., 2003. The effect of 10% HF treatment on the resolution of CPMA 13C NMR spectra and on the quality of organic matter in Ferralsols. *Geoderma* 116, 373-392.

Gordien, A.Y., Gray, A.I., Franzblau, S.G., Seidel, V., 2009. Antimycobacterial terpenoids from *Juniperus communis* L. (Cupressaceae). *Journal of Ethnopharmacology* 126, 500-505.

Kaal, J., Mailänder, S., 2018. Molecular properties of soil organic matter in dark buried colluvium from South Germany show abundance of fire residues from Early Neolithic vegetation clearance and slash and burn agriculture. *Analytical Pyrolysis Letters* APL004, 1-10 (www.pyrolyscience.com/apl004/).

Kaal, J., Rumpel, C., 2009. Can pyrolysis-GC/MS be used to estimate the degree of thermal alteration of black carbon?

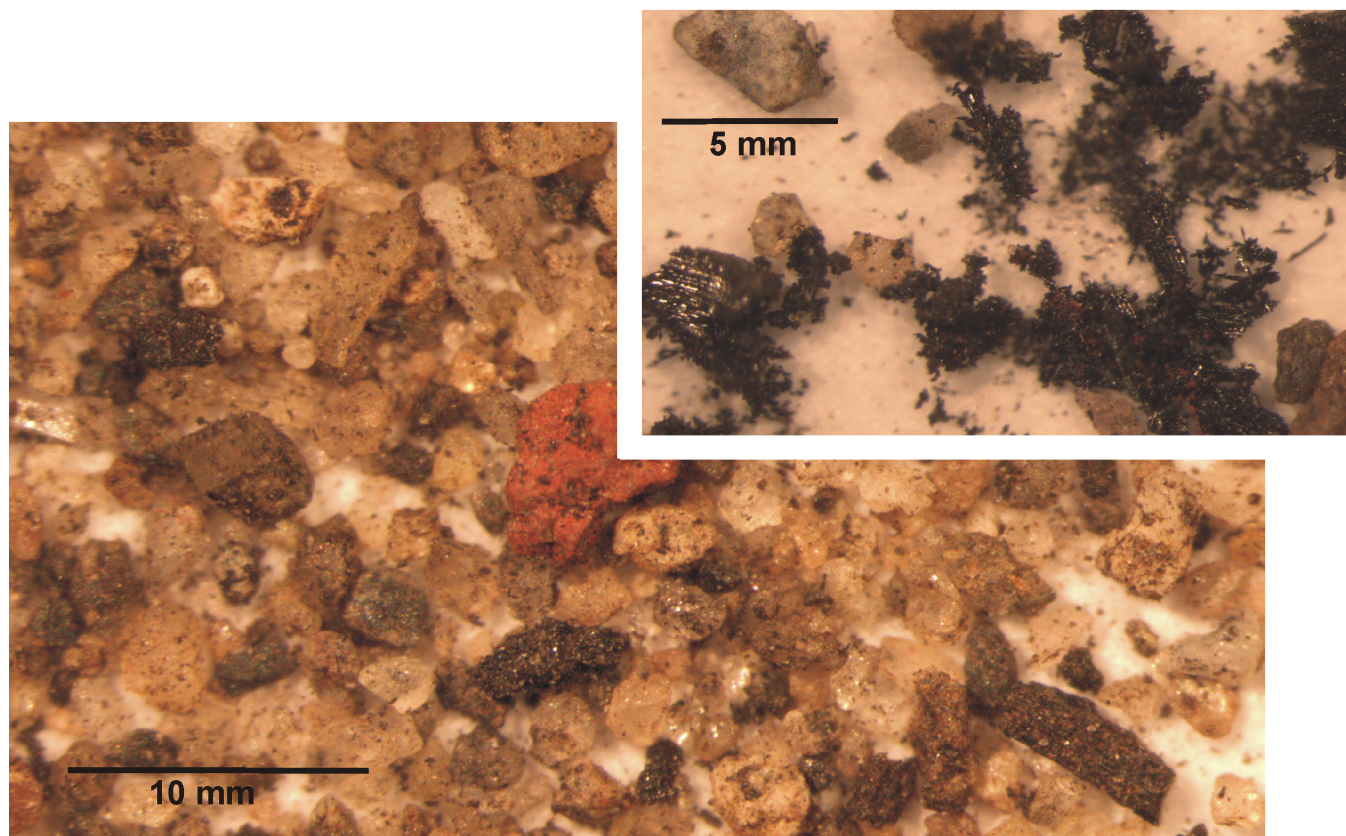


Fig. 5. Photograph of pyrogenic OM (black carbon) particles from the sample obtained at 45 cm depth.

Organic Geochemistry 40, 1179-1187.

Kaal, J., Brodowski, S., Baldock, J.A., Nierop, K.G.J., Martínez Cortizas, A., 2008a. Characterisation of aged black carbon using pyrolysis-GC/MS, thermally assisted hydrolysis and methylation (THM), direct and cross polarisation ^{13}C nuclear magnetic resonance (DP/CP NMR) and the benzene polycarboxylic acid (BPCA) method. *Organic Geochemistry* 39, 1415-1426.

Kaal, J., Martínez Cortizas, A., Nierop, K.G.J., Buurman, P., 2008b. A detailed pyrolysis-GC/MS analysis of a black carbon-rich acidic colluvial soil (Atlantic ranker) from NW Spain. *Applied Geochemistry*, 23, 2395-2405.

Kaal, J., Nierop, K.G.J., Martínez Cortizas, A., 2009. Characterisation of aged charcoal using a coil probe pyrolysis-GC/MS method optimised for black carbon. *Journal of Analytical and Applied Pyrolysis* 85, 408-416.

Kaal, J., López Costas, O., Martínez Cortizas, A., 2016. Diagenetic effects on pyrolysis fingerprints of extracted collagen in archaeological human bones from NW Spain, as determined by pyrolysis-GC-MS. *Journal of Archaeological Science*. 65, 1-10.

Kaal, J., Gianotti, C., del Puerto, L., Criado Boado, F., Rivas, M., 2019. Molecular features of organic matter in anthropogenic earthen mounds, canals and lagoons in the Pago Lindo archaeological complex (Tacuarembó, Uruguayan lowlands) are controlled by pedogenetic processes and fire practices. *Journal of Archaeological Science: Reports*. 29, 103100.

Kögel-Knabner, I., Rumpel, C., 2018. Advances in molecular approaches for understanding soil organic matter composition, origin, and turnover: A historical overview. *Advances in Agronomy* 149, 1-48.

Larsson, T.B., 2010. Människan och älgen vid Bastuloken:

En delundersökt boplatzvall från neolitikum i Västernorrland. *Arkeologii Norr*. 12, 1-16. Umeå universitet.

Larsson, T.B., Rosqvist, G., Ericsson, G., Heinerud, J., 2012. Climate Change, Moose and Humans in Northern Sweden 4000 cal. yr BP. *Journal of Northern Studies*, 6(1), 9-30.

Linderholm, J., Fernández Pierna, J.A., Vincke, D., Dardenne, P., Baeten, V., 2013. Identification of fragmented bones and their state of preservation using near infrared hyperspectral image analysis. *Journal of Near Infrared Spectroscopy*, 21, 459-466.

Linderholm, J., Geladi, P., Gorretta, N., Bendoula, R., Gobrecht, A., 2019. Near infrared and hyperspectral studies of archaeological stratigraphy and statistical considerations. *Geochronology* 2019, 1-11, doi: 10.1002/gea.21731.

Marbot, R., 1997. The selection of pyrolysis temperatures for the analysis of humic substances and related materials. 1. Cellulose and chitin. *Journal of Analytical and Applied Pyrolysis* 39, 97-104.

Mills, J.S., White, R., 1994. *The organic chemistry of museum objects* (Second edition). Butterworth-Heinemann, London, pp. 102-103.

Miltner, A., Zech, W., 1997. Effects of minerals on the transformation of organic matter during simulated fire-induced pyrolysis. *Organic Geochemistry* 26, 175-182.

Nierop, K.G.J., van Bergen, P.F., 2002. Clay and ammonium catalyzed reactions of alkanols, alkanolic acids and esters under flash pyrolytic conditions. *Journal of Analytical and Applied Pyrolysis* 63, 197-208.

Nierop, K.G.J., van Bergen, P.F., Buurman, P., van Lagen, B., 2005. NaOH and Na₄P₂O₇ extractable organic matter in two allophanic volcanic ash soils of the Azores Islands—a pyrolysis

GC/MS study. *Geoderma* 127, 36-51.

Peris Vicente, J., 2008. Estudio analítico de materiales empleados en barnices, aglutinantes y consolidantes en obras de arte mediante métodos cromatográficos y espectrométricos. PhD Thesis. Universitat de València, pp. 286.

Poirier, N., Sohi, S.P., Gaunt, J.L., Mahieu, N., Randall, E.W., Powlson, D.S., Evershed, R.P., 2005. The chemical composition of measurable soil organic matter pools. *Organic Geochemistry* 36, 1174-1189.

Pouwels, A.D., Eijkel, G.B., Boon, J.J., 1989. Curie-point pyrolysis-capillary gas chromatography-high-resolution mass spectrometry of microcrystalline cellulose. *Journal of Analytical and Applied Pyrolysis* 14, 237-280.

Ross, A.B., Junyapoon, S., Jones, J.M., Williams, A., Bartle, K.D., 2005. A study of different soots using pyrolysis-GC-MS and comparison with solvent extractable material. *Journal of Analytical and Applied Pyrolysis* 74, 494-501.

Rumpel, C., González-Pérez, J.A., Bardoux, G., Largeau, C., González-Vila, F.J., Valentin, C., 2007. Composition and reactivity of morphologically distinct charred materials left after slash-and-burn practices in agricultural tropical soils. *Organic Geochemistry* 38, 911-920.

Sáiz-Jiménez, C., 1995. Production of alkylbenzenes and alkyl-naphthalenes upon pyrolysis of unsaturated fatty acids. A model reaction to understand the origin of some pyrolysis products from humic substances? *Naturwissenschaften* 81, 451-453.

Schellekens, J., Buurman, P., Pontevedra-Pombal, X., 2009. Selecting parameters for the environmental interpretation of peat molecular chemistry - A pyrolysis-GC/MS study. *Organic Geochemistry* 40, 678-691.

Schnitzer, M., Kodama, H., Schulten, H.-R., 1994. Mineral effects on the pyrolysis-field ionization mass spectrometry of fulvic acid. *Soil Science Society of America Journal* 58, 1100-1107.

Schnitzer, M.I., Monreal, C.M., Jandl, G., Leinweber, P., Franscham, P.B., 2007. The conversion of chicken manure to biooil by fast pyrolysis II. Analysis of chicken manure, biooils, and char by curie-point pyrolysis-gas chromatography/mass spectrometry (Cp Py-GC/MS). *Journal of Environmental Science and Health Part B* 42, 79-95.

Sharp, H., Latif Z., Bartholomew, B., Bright, C., Jones, C.D., Sarker, S.D., Nash, R.J., 2001. Totarol, totaradiol and ferruginol: three diterpenes from *Thuja plicata* (Cupressaceae). *Biochemical Systematics and Ecology* 29, 215-217.

Shedrinsky, A.M., Wampler, T.P., Indictor, N., Baer, N.S., 1989. Application of analytical pyrolysis to problems in art and archaeology: a review. *Journal of Analytical and Applied Pyrolysis* 15, 393-412.

Smith, G.G., Reddy, G.S., Boon, J.J., 1988. Gas chromatographic-mass spectrometric analysis of the Curie-point pyrolysis products of some dipeptides and their diketopiperazine. *Journal of the Chemical Society, Perkin Transactions* 2, 203-211.

Song, J., Peng, P., 2010. Characterisation of black carbon materials by pyrolysis-gas Chromatography-mass spectrometry. *Journal of Analytical and Applied Pyrolysis* 87, 129-137.

Song, X., Farwell, S.O., 2004. Pyrolysis gas chromatography atomic emission detection method for determination of N-containing components of humic and fulvic acids. *Journal of Analytical and Applied Pyrolysis* 71, 901-915.

Stankiewicz, B.A., van Bergen, P.F., Duncan, I.J., Carter, J.F., Briggs, D.E.G., Evershed, R.P., 1996. Recognition of chitin and proteins in invertebrate cuticles using analytical pyrolysis/gas

chromatography and pyrolysis/gas chromatography/mass spectrometry. *Rapid Communications in Mass Spectrometry* 10, 1747-1757.

Stankiewicz, B.A., Hutchins, J.C., Thomson, R., Briggs, D.E.G., Evershed, R.P., 1997. Assessment of bog-body tissue preservation by pyrolysis-gas chromatography/mass spectrometry. *Rapid Communications in Mass Spectrometry* 11, 1884-1890.

Stankiewicz, B.A., Mastalerz, M., Hof, C.H.J., Bierstedt, A., Flannery, M.B., Briggs, D.E.G., Evershed, R.P., 1998. Biodegradation of the chitin-protein complex in crustacean cuticle. *Organic Geochemistry* 28, 67-76.

Storå, J., Strand, L., Fridén-Rolstadaas, M., 2011. Osteological analysis of unburnt and burnt skeleton findings from the Stone Age site Bastuloken, Raå 183, Ramsele parish, County of Västernorrland. Rapport 2011:10, Osteologiska forskningslaboratoriet, Stockholm University.

Suárez-Abelenda, M., Buurman, P., Camps, M., Kaal, J., Martínez Cortizas, A., Gartzia, N., Macías, F., 2011. Comparing NaOH-extractable organic matter of acid forest soils that differ in their pedogenic trends: a pyrolysis-GC/MS study. *European Journal of Soil Science* 62, 834-848.

Suárez-Abelenda, M., Kaal, J., McBeath, V., 2017. Translating analytical pyrolysis fingerprints to Thermal Stability Indices (TSI) to improve biochar characterization by pyrolysis-GC-MS. *Biomass and Bioenergy* 98, 306-320.

Van Bergen, P., Flannery, M.B., Poulton, P.R., Evershed, R.P., 1998. Organic geochemical studies of soils from Rothamsted experimental station. III. Nitrogen-containing organic matter in soil from Geescroft Wilderness. In: Stankiewicz, B.A., van Bergen, P.F. (Eds.), *Fate of N-containing macro molecules in the bio- and geosphere*. American Chemical Society Symposium Series 707, 321-338.

Van der Kaaden, A., Boon, J.J., de Leeuw, J.W., de Lange, F., Schuyf, P.W.J., Schulten, H.-R., Bahr, U., 1984. Comparison of analytical pyrolysis techniques in the characterization of chitin. *Analytical Chemistry* 56, 2160-2165.

Zegouagh, Y., Derenne, S., Dignac, M.F., Baruiso, E., Mariotti, A., Largeau, C., 2004. Demineralisation of a crop soil by mild hydrofluoric acid treatment: Influence on organic matter composition and pyrolysis. *Journal of Analytical and Applied Pyrolysis* 71, 119-135.

Table 1. List of pyrolysis products and source allocation (CARB=carbohydrate, MAH=monocyclic aromatic hydrocarbon, MCC=methylene chain compound, NCOMP=N-compound, PAH=polycyclic aromatic hydrocarbon, PHEN=phenol). Labels refer to peak labels in the example chromatograms of Figure 1.

Label	RT (min)	Compound	<i>m/z</i>	group
1	1.855	C ₆ -alkene	55+56	MCC
2	2.145	benzene	78	MAH
3	2.612	<i>N</i> -methylpyrrole	81+80	NCOMP
4	2.727	pyridine	79+52	NCOMP
5	2.768	pyrrole	67	NCOMP
6	2.809	toluene	91+92	MAH
7	3.370	3/2-furaldehyde	95+96	CARB
8	3.391	C ₈ -alkene	70+55	MCC
9	3.479	C ₁ -pyrrole	80+81	NCOMP
10	3.593	C ₂ -benzene	91+106	MAH
11	3.811	C ₉ -alkene	55+69	MCC
12	3.822	C ₉ -alkane	57+71	MCC
13	3.837	acetamide	59	NCOMP
14	3.878	styrene	104+78	MAH
15	3.894	C ₂ -benzene	91+106	MAH
16	4.594	5-methyl-2-furaldehyde	110+109	CARB
17	4.693	C ₁₀ -alkene	55+69	MCC
18	4.760	C ₁₀ -alkane	57+71	MCC
19	4.807	benzotrile	103+76	NCOMP
20	4.984	phenol	94+66	PHEN
21	5.004	4-hydroxy-5,6-dihydro-(2 <i>H</i>)-pyran-2-one	114+58	CARB
22	5.253	indene	115+116	PAH
23	5.352	dianhydrorhamnose	128+113	CARB
24	5.518	C ₁₁ -alkene	55+69	MCC
25	5.539	C ₁ -phenol	108+107	PHEN
26	5.596	C ₁₁ -alkane	57+71	MCC
27	5.684	guaiacol	109+124	LIGNIN
28	5.726	4-methylphenol	108+107	PHEN
29	5.918	levoglucosenone	68+98	CARB
30	6.110	C ₁ -benzotrile	117+90	NCOMP
31	6.130	C ₁ -indene	130+115	PAH
32	6.250	C ₂ -phenol	107+122	PHEN
33	6.312	C ₁₂ -alkene	55+69	MCC
34	6.369	C ₁₂ -alkane	57+71	MCC
35	6.431	2-carbonitrilepyrrole	92+65	NCOMP
36	6.447	naphthalene	128	PAH

Continued on next page

Continued from previous page

Label	RT (min)	Compound	<i>m/z</i>	group
37	6.499	4-methylguaiacol	123+138	LIGNIN
38	6.608	unidentified carbohydrate	69+57	CARB
39	6.800	unidentified N-containing compound	95	NCOMP
40	6.820	1,4:3,6-dianhydro- α -D-glucopyranose	69+57	CARB
41	7.038	C ₁₃ -alkene	55+69	MCC
42	7.090	C ₁₃ -alkane	57+71	MCC
43	7.272	C ₁ -naphthalene	142+115	PAH
44	7.373	indole	117+90	NCOMP
45	7.401	C ₁ -naphthalene	142+115	PAH
46	7.401	4-vinylguaiacol	150+135	LIGNIN
47	7.635	4 <i>H</i> -trimethylnaphthalene	159+177	PAH
48	7.671	C ₃ -guaiacol	164+149	LIGNIN
49	7.733	C ₁₄ -alkene	55+69	MCC
50	7.775	C ₁₄ -alkane	57+71	MCC
51	7.832	biphenyl	154+153	PAH
52	8.014	C ₃ -guaiacol	164+149	LIGNIN
53	8.019	C ₂ -naphthalene	156+141	PAH
54	8.149	4-formylguaiacol	151+152	LIGNIN
55	8.320	C ₃ -guaiacol	164+149	LIGNIN
56	8.392	C ₁₅ -alkene	55+69	MCC
57	8.413	C ₁₅ -alkane	57+71	MCC
58	8.699	4-acetylguaiacol	151+166	LIGNIN
59	8.787	dibenzofuran	168+139	PAH
60	8.989	C ₁₆ -alkene	55+69	MCC
61	9.031	C ₁₆ -alkane	57+71	MCC
62	9.197	fluorene	165+166	PAH
63	9.321	levoglucosan	60+73	CARB
64	9.586	C ₁₇ -alkene	55+69	MCC
65	9.601	C ₁₇ -alkane	57+71	MCC
66	9.783	prist-1-ene	55+56	MCC
67	10.011	diketodipyrrole	186+93	NCOMP
68	10.115	C ₁₈ -alkene	55+69	MCC
69	10.151	C ₁₈ -alkane	57+71	MCC
70	10.260	unidentified N-containing compound	171+172	NCOMP
71	10.354	unidentified aliphatic	82+95	MCC
72	10.374	unidentified aliphatic	67+68	MCC
73	10.385	phenanthrene/anthracene	178	PAH
74	10.566	unidentified N-containing compound	200+199	NCOMP
75	10.639	unidentified N-containing compound	185	NCOMP

Continued on next page

Continued from previous page

Label	RT (min)	Compound	<i>m/z</i>	group
76	10.644	C ₁₉ -alkene	55+69	MCC
77	10.681	C ₁₉ -alkane	57+71	MCC
78	10.686	unidentified N-containing compound	176+154	NCOMP
79	10.722	triazoloquinoline compound	200+199	NCOMP
80	10.738	unidentified aliphatic	81+95	MCC
81	10.748	C ₁₆ -nitrile	97+110	NCOMP
82	11.137	C ₁₆ -fatty acid	60+73	MCC
83	11.303	2,5-diketopiperazine	70+194	NCOMP
84	11.635	C ₂₁ -alkene	55+69	MCC
85	11.651	C ₂₁ -alkane	57+71	MCC
86	11.734	C ₁₈ -nitrile	97+110	NCOMP
87	12.030	C ₂₂ -alkene	55+69	MCC
88	12.030	C ₁₈ -fatty acid	60+73	MCC
89	12.092	C ₂₂ -alkane	57+71	MCC
90	12.175	C ₁₆ -amide	59+72	NCOMP
91	12.491	C ₂₃ -alkene	55+69	MCC
92	12.528	C ₂₃ -alkane	57+71	MCC
93	12.787	unidentified compound	83+280	OTHER
94	12.823	totarol	271+175	OTHER
95	12.891	C ₂₀ -fatty acid	60+73	MCC
96	12.922	C ₂₄ -alkene	55+69	MCC
97	12.948	C ₂₄ -alkane	57+71	MCC
98	13.041	C ₁₈ -amide	59+72	MCC
99	13.332	C ₂₅ -alkene	55+69	MCC
100	13.342	C ₂₅ -alkane	57+71	MCC
101	13.431	C ₂₃ -methylketone	58+59	MCC
102	13.685	C ₂₂ -fatty acid	60+73	MCC
103	13.711	C ₂₆ -alkene	55+69	MCC
104	13.716	C ₂₆ -alkane	57+71	MCC
105	13.820	C ₂₄ -methylketone	58+59	MCC
106	14.090	C ₂₇ -alkene	55+69	MCC
107	14.090	C ₂₇ -alkane	57+71	MCC
108	14.183	C ₂₅ -methylketone	58+59	MCC
109	14.442	C ₂₈ -alkane	57+71	MCC
110	14.448	C ₂₈ -alkene	55+69	MCC
111	14.557	C ₂₆ -methylketone	58+59	MCC
112	14.795	C ₂₉ -alkane	57+71	MCC
113	14.800	C ₂₉ -alkene	55+69	MCC
114	14.904	C ₂₇ -methylketone	58+59	MCC

Continued on next page

Continued from previous page

Label	RT (min)	Compound	<i>m/z</i>	group
115	15.127	C ₃₀ -alkane	57+71	MCC
116	15.132	C ₃₀ -alkene	55+69	MCC
117	15.247	C ₂₈ -methylketone	58+59	MCC
118	15.496	C ₃₁ -alkene	55+69	MCC
119	15.501	C ₃₁ -alkane	57+71	MCC
120	15.605	C ₂₉ -methylketone	58+59	MCC
121	15.807	stigmasta compound	396+147	MCC
122	15.869	C ₃₂ -alkene	55+69	MCC
123	15.874	C ₃₂ -alkane	57+71	MCC
124	16.295	C ₃₃ -alkane	57+71	MCC
125	16.456	C ₃₁ -methylketone	58+59	MCC
126	17.426	stigmasta compound	174+410	MCC
127	17.768	stigmasta compound	409+441	MCC